246 (2025) 213662

Contents lists available at ScienceDirect

Geoenergy Science and Engineering

journal homepage: www.sciencedirect.com/journal/geoenergy-science-and-engineering

Modeling and analysis of hydrodynamic and pressure force for flow-induced vibration on an elbow in a gas-liquid system

C. Garcia [a,*], C. Nogueira Sondermann [a], E. Pereyra [a], L. Korelstein [b], C. Sarica [a]

[a] McDougall School of Petroleum Engineering, The University of Tulsa, Tulsa, OK, 74104, United States
[b] Piping Systems Research & Engineering Co, Montenegro

ARTICLE INFO

Keywords:
Hydrodynamic force
Pressure pulsation
Flow-induced force
Flow-induced vibration
Multiphase flow
Flow pattern
Slug
Pseudo-slug
Flow density
Flow velocity

ABSTRACT

Flow-induced vibration (FIV) is studied on a horizontal 90-degree elbow in this paper. It was noted that the slugs and pseudo-slugs on the elbow cause the maximum force. Particularly, pseudo-slug flow in gas-liquid systems results in higher force amplitude peaks. These high force amplitudes may potentially cause fatigue in elbows due to the occurrence of flow-induced vibration. Pseudo-slug flow pattern occurs in the transition from slug to segregated flows. It was identified that the magnitude of the force fluctuation is influenced by the change in momentum flux and pressure. Thus, the pressure force can be interpreted as the base from which the hydrodynamic forces create the overall force peaks. Analysis of time-varying quantities of the liquid holdup (slug liquid holdup, 0.18 to 1.00), flow-induced force (force peaks, 10–620 N), and pressure pulsation (pressure fluctuation, 2500–35000 Pa) allowed the study of the separate contributions of momentum and pressure terms on the magnitude of the force fluctuation (force amplitude, 4–180 N). The findings indicate that pressure fluctuations within the elbow play a significant role in estimating force magnitude in pseudo-slug flow, whereas they are not predominant in slug flow. Based on the analysis, a mechanistic model capable of predicting the impacting force as a function of the flow pattern and operational conditions is proposed.

1. Introduction

Intermittent flow, such as slug or pseudo-slug flow, induces cyclic stresses in pipe systems. According to Yih and Griffith (1968), intermittent flow is accompanied by fluctuations in interrelated variables such as pressure, liquid holdup, and momentum flux. Also, understanding the nature of these cyclic stresses is vital in determining the fatigue life of a piping structure. The two critical parameters to determine the fatigue of piping systems due to multiphase flow are a) the range of stress or the magnitude of the force peaks caused by the impact of such structures on the accessories (i.e., elbows) and b) the frequency of fluid structures with higher density and velocity (i.e., slug or pseudo-slug bodies).

The influence of different flow patterns on the hydrodynamic force magnitude and frequency measurements has been studied by Garcia et al. (2023a) on a horizontal to horizontal elbow. Later, a slug frequency correlation was developed to improve the predictivity in high-frequency conditions, which are relevant in fatigue analysis (Garcia et al., 2023b). In the case of the peak force magnitude, the main observation is the linear influence of the structure velocity (v_S) on the magnitude of the force peaks as flow changes from slug to pseudo-slug flow. The velocity of the slug or pseudo-slug body region is the structure velocity associated with the momentum flux inducing the force peaks.

The structure velocity is linearly dependent on the mixture velocity for slug flow; thus, given a constant superficial liquid velocity (v_{SL}), increasing the superficial gas velocity (v_{SG}), and consequently, the mixture velocity ($v_M = v_{SL} + v_{SG}$), will result in a proportional increase in translational velocity (Shoham, 2006). However, as the gas flow rate further increases, the flow pattern changes from slug to pseudo-slug. A continuous gas passage through the slug body characterizes this flow pattern. Pseudo-slug (PSL) is described as the transition between the conventional slug (SL) and segregated flows (stratified ST and annular ANN). PSL flow exhibits lower structure velocity than the expected linear increase for SL flow.

On the other hand, the film region's influence over the hydrodynamic force seems minimal, with values close to zero and independent of the liquid holdup. Conversely, the flow and hitting of slug/pseudo-slugs, with structure density (ρ_S), cause the force peaks (Garcia et al., 2023a). Therefore, the force magnitude could be associated with the influence of

* Corresponding author.
E-mail addresses: ceg9863@utulsa.edu, cesar.garcia6@woodplc.com (C. Garcia).

https://doi.org/10.1016/j.geoen.2025.213662
Received 1 October 2024; Received in revised form 4 December 2024; Accepted 2 January 2025
Available online 3 January 2025

the maximum values of momentum flux ($\rho_S v_S^2$).

From the experimental observations reported by Garcia et al. (2023a), the force term associated with the momentum flux ($\rho_S v_S^2 A$) shows a fair agreement with the hydrodynamic force measured for the slug flow pattern. However, it can be found that for pseudo-slug flow, high force values were measured on the elbow no matter if the PSL bodies have less density and relatively less structure velocity (consequently less momentum flux) than the slug flow patterns (Garcia et al., 2023a). This could be explained by the influence of high fluctuations in pressure. Thus, the influence of both momentum and pressure terms is relevant for pseudo-slug flow.

Tay and Thorpe (2014) have proposed a flow model to predict the time-dependent forces acting on horizontal pipe bends in slug flow, including momentum and pressure terms. Their model was validated with experimental data for air-water slug flow. They noticed that the force trace increases abruptly when the liquid slug enters the pipe bend. When the liquid slug exits the bend, the force drops rapidly, although not as steeply as when it enters the bend. Additionally, a better agreement with the model prediction was observed at the front of the liquid slug. However, a dip occurred during the transit of the liquid slug body, where the model predicts an incremental force due to the progressive pressure increase (Tay and Thorpe, 2014).

Liu et al. (2012) developed a two-phase flow-induced excitation force model. The impact of liquid slugs could induce instantaneous shock in micro to milliseconds and impose a pressure impulse on the elbow. However, it is mentioned that the major force fluctuations should be caused by the momentum flux fluctuations (Liu et al., 2012). Miwa and Hibiki (2020) explained those fluctuations by considering possible water hammer effects (pressure spikes of extremely short duration).

Klinkenberg and Tijsseling (2021) proposed a stochastic mechanistic model for the slug force acting on a pipe bend. The lengths of individual slug zones in the train are randomly selected from a probability distribution function. The fluctuating slug flow quantities (liquid holdup and fluid velocities) are then estimated with a slug model. Force on the bend was calculated with a momentum balance equation. The prediction trend was good for all tested pipe diameters and fluid properties, except for flow cases in the slug-annular transition region (Klinkenberg and Tijsseling, 2021).

Fig. 1 represents the force on the bend and the contributions of momentum and pressure based on the model solution (Klinkenberg and Tijsseling, 2021).

With the arrival of the slug body to the bend, a sudden increase in the force is expected due to the momentum flux terms. Then, a progressive influence of pressure causes an additional incremental force through movement from the nose to the tail of each slug. After the passage of the slug body, the force trace would be equivalent to the pressure term returning at low values during the film region flow.

In the present work, the force peak magnitude was measured on a single horizontal elbow (90-degree) to identify which flow parameters affect the force in slug and pseudo-slug flows most. Time signatures of the upstream liquid holdup, upstream pressure, downstream pressure, and structural reaction force were synchronized to evaluate the influence of local pressure fluctuations on the force magnitude. This study uses mineral oil with a density of 800 kg/m^3 and a viscosity of 6 cp at 80 °F as a liquid phase to better represent field conditions. Experimental observations and findings revealed that the magnitude of the force is influenced by the change in momentum flux and pressure. The results show that pressure fluctuations in the elbow are significant for estimating the force magnitude in pseudo-slug flow, whereas it is not significant for slug flow conditions. The proposed mechanistic model is based on these observations.

2. Experimental setup

This section describes the experimental facility and instrumentation utilized for this study. Garcia et al. (2023a) present more details of the experimental setup. A TUFFP multiphase flow loop, which has been used for a wide range of liquid viscosity fluids, is coupled with a force system to evaluate flow-induced vibrations. The setup developed for the present study could be used for further evaluations with fluids of different properties.

2.1. Multiphase loop and force characterization system

The 50.8-mm ID horizontal oil/gas two-phase experimental flow loop of the Tulsa University Fluid Flow Projects (TUFFP) is used in this study (see schematic in Fig. 2). One pair of capacitance sensors (CP1 and CP2) is used to analyze the slug characteristics. High-quality pressure sensors (HQP) are installed to evaluate the influence of pressure on the

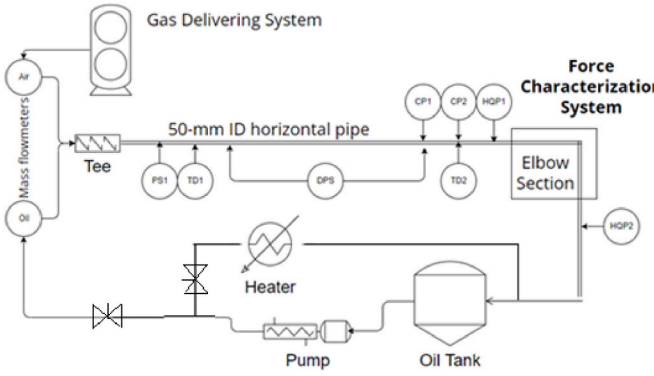

Fig. 2. Schematic of the experimental facility.

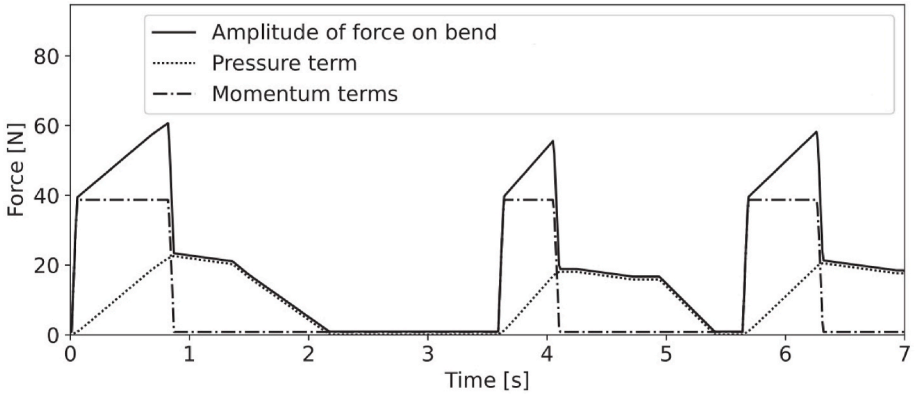

Fig. 1. Total force amplitude and a split into momentum and pressure contribution (Klinkenberg and Tijsseling, 2021).

forces in the elbow system.

The force characterization system is installed to evaluate FIV on a horizontal elbow at the end of the straight horizontal pipe. After the elbow, a return line, approximately 25 m in length, leads the fluids to the oil tank. Fig. 3 shows a perspective of the force characterization system. The elbow section comprises two pieces of clear PVC pipes (50.8-mm ID, 0.5 m long) connected to a 90° elbow (radius 50.8 mm, R/D = 1.0). The use of transparent pipes helps identify flow patterns, and it could be adapted to apply computer vision techniques in the future. The elbow section is loosely attached to the upstream and downstream piping by two 0.1 m long flexible corrugated pipes. The corrugated pipes allow the measurement of the hydrodynamic force without the influence of the piping structure.

The elbow is fixed to the upper surface of a thin metal plate. Two triaxial dynamic force sensors (TecGihan USL06-H5-500 N) are installed diagonally under the thin plate. The input flow direction to the elbow was used as the X-axis on the force sensors, and the output flow direction from the elbow was the Y-axis on the force sensors.

2.2. Fast response pressure sensors

Two high-speed pressure sensors (HQP1 and HQP2) are installed before and after the elbow to obtain high-speed pressure data and characterize the hydrodynamic peak force by subtracting the pressure force from the overall force measurements and evaluating the influence of pressure variation $\Delta P(t)$ on the magnitude of FIV under the elbow. The HQP transducers are located symmetrically at 0.95 m from the elbow.

2.3. Capacitance sensors

Two capacitance sensors, based on the dielectric constants of air and oil, are installed before the elbow to measure in-situ liquid holdup and the velocity of flow structures. The sensors have been calibrated using the procedure proposed by Brito (2012). A calibration curve is built using a set of quick-closing valves. The calibration curve is utilized to convert dimensionless voltages into liquid holdup values. The capacitance sensors are located at 3.01 m before the elbow.

2.4. Other instrumentation and data acquisition system

During the experiments, a data acquisition system monitors pressure, temperature, flow rates, output voltage from capacitance sensors, and mass gas and liquid flow rates. This system comprises a PC, a multifunction I/O board, and the LabVIEW™ software package. The output voltage from the force sensors is acquired with another data acquisition system, including a laptop, an amplifier, and the LabVIEW™ software package. All data files have TDMS format with a total test time of at least 1 min. The high-speed data acquisition system has a rate of 1000 samples per second. Instrument systematic uncertainties are included for flow rates, densities, temperature, and pressure. Further studies could include improved experimental setup by using additional FIV measurement techniques as displacement dials, accelerometers, or string gauges.

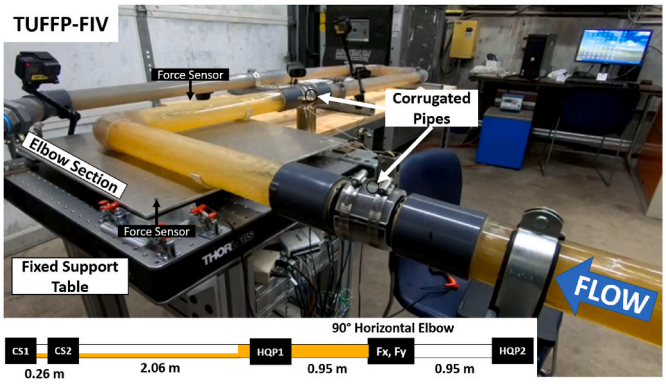

Fig. 3. TUFFP-FIV system, perspective, and sensor distance.

2.5. Fluid and operational conditions

Light yellow low-viscosity mineral oil was used as the liquid phase during the experiments. Its viscosity and density were characterized using a dynamic rheometer and single-phase oil runs. Table 1 shows the oil properties at 80 °F. The viscosity and density are correlated for flow analysis following the recommended practices (ASTM D341-09, 2015, Gottfried, 1965).

The flow pattern map was generated for the current fluid properties and pipe geometry using Barnea's model (Barnea, 1987), as presented in Fig. 4. A wide range of liquid and gas superficial velocities were studied (v_{SL} 0.1–2.5 m/s, v_{SG} 1–10 m/s). The following flow patterns were obtained: slug flow (SL), pseudo-slug (PSL), and annular flow (ANN or A). The transitions to dispersed bubble (DB) and stratified (ST or SS) are also identified. All the flow conditions marked in Fig. 4 were repeated three times.

3. Experimental results

The data collected from the experimental facility was processed to obtain the velocity and density of the structures (slugs, pseudo-slugs, or waves) and the peak force parameters (frequency and magnitude). This data analysis provides the input variables for calculating the hydrodynamic force related to the magnitude of force peaks. The results are compared with force and pressure measurements to identify the most relevant variables.

Uncertainty analysis provides confidence in the quality of the experimental data (Dieck, 2007). It includes estimating the combined random and systematic uncertainties for recorded parameters (pressure, temperature, mass flow rates) and the estimation of uncertainty propagation on study variables (liquid density, gas density, superficial liquid velocity, superficial gas velocity, and mixture velocity). Brito (2012) provided more details on the uncertainty calculation. The propagated uncertainty is lower than 2% for all the study variables.

The following section separates the results into two parts: 1) characterization of flow structure velocity and liquid holdup (quantities associated with the momentum flux, ρv^2) 2) synchronization of flow-structure signal with force and pressure signatures to identify the influence of pressure fluctuation on the magnitude of the force peaks.

3.1. Structure velocity (v_S) and liquid holdup (H_L)

Flow structures, such as slugs, pseudo-slugs, or waves, move at a specific velocity (v_S) calculated by a cross-correlation procedure to determine the time delay between two consecutive CP sensors (in milliseconds). Fig. 5 shows a data sample (time interval between 30.000 and 35.000 ms) of a flow structure monitored with the CP sensors for slug flow.

Fig. 6 shows the flow structure velocity measurements for all the experimental repetitions. The results in the data point represent the mean value obtained for the repetitions, and the error bars are their standard deviation. For low v_{SL} conditions (0.1 and 0.2 m/s), there are

Table 1
Properties of mineral oil.

Viscosity, μ_L	Density, ρ_L	Surface tension, σ	Color
(mPa•s)	(kg/m^3)	(N/m)	(–)
6.2 @ 80 °F	798 @ 80 °F	0.023	Light yellow

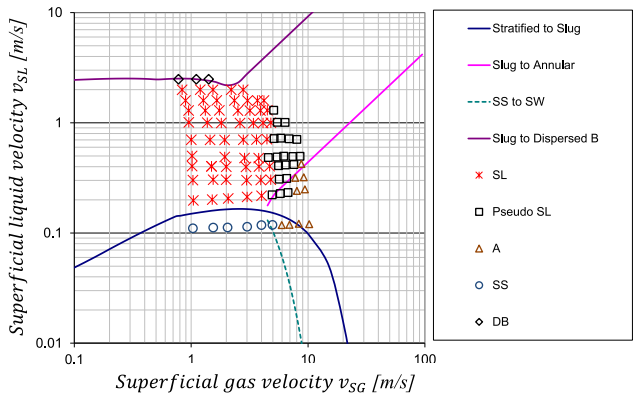

Fig. 4. Experimentally observed flow patterns on top of Barnea's (1987) map.

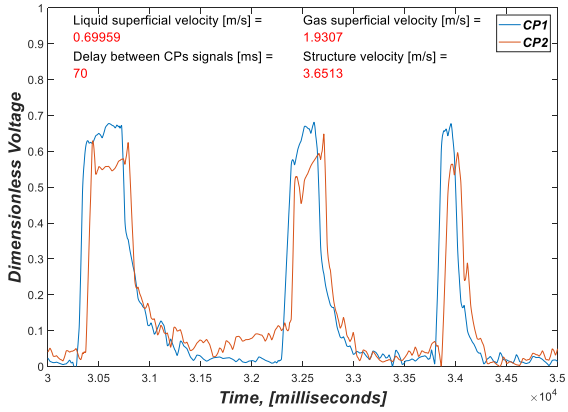

Fig. 5. Sample of slug flow structure monitoring ($\Delta t = 5\,s$).

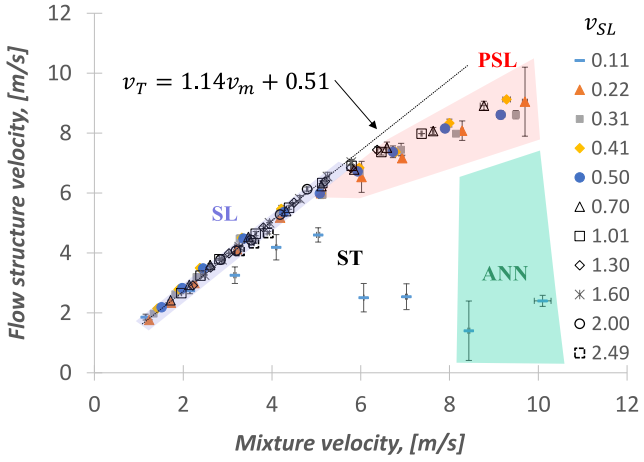

Fig. 6. Flow structure velocity (v_S).

some conditions with moderate variation (high standard deviation between repetitions). On the other conditions with less variation ($v_{SL} \geq$ 0.3 m/s), the structure velocity increases linearly with a characteristic slope with the increase of mixture velocity. This slope reduces for a mixture velocity of around 5 m/s.

PSLs exhibit lower flow structure velocity than the expected linear increase for SLs. For wavy annular flow (ANN) at low liquid (v_{SL} <0.2 m/s) and high gas flow rates (v_{SG} >7.0 m/s), the liquid film thickness is low, and liquid is swept up and around the pipe, creating a liquid-film annulus. Finally, at $v_{SL} = 0.1$ m/s, the flow is stratified (ST) with some waves moving at low velocities. The herein work mainly focuses on intermittent flow patterns: Slug (SL) and Pseudo-slug (PSL).

The characterization of flow structures such as slugs or pseudo-slugs is performed by monitoring the in-situ liquid holdup (H_L), using the capacitance probes. With this information and using the oil and gas densities, it is possible to calculate the density in the slug/pseudo-slug bodies with high average holdup values. For the slug flow pattern, the structure density includes the slug body holdup (H_{LLS}) as follow:

$$\rho_S = \rho_L H_{LLS} + \rho_G(1 - H_{LLS}) \tag{1}$$

The expected hydrodynamic force associated with momentum flux would be the difference between momentum flux flor slug and film regions:

$$F_H = (\rho_S v_S^2 - \rho_F v_F^2)A \tag{2}$$

The analysis of hydrodynamic forces has shown that the film region's influence is minimal and independent of the liquid holdup fraction (Garcia et al., 2023a). In addition, Figs. 7 and 8 show the liquid holdup, density, and momentum flux for slug and pseudo-slug flows. Central values for these variables of interest in the shown cases are: for the slug condition: $H_{LLS} = 0.78$, $\rho_S = 618$ kg/m^3, $\rho_S v_S^2 A = 16.7$ N; for the pseudo-slug condition: $H_{LLS} = 0.38$, $\rho_S = 289$ kg/m^3, $\rho_S v_S^2 A = 45.4$ N

The results indicate that pseudo-slugs (Fig. 8) are extremely aerated structures generated by the gas penetration into the pseudo-slug body, differently from slug flow (Fig. 7), in which the slug body occupies the entire pipe cross-section. Based on the time-series liquid holdup data from the capacitance sensor, PSL shows an inverted V-shape rise that indicates the amount of liquid present in the cross-section of the pipe.

3.2. Pressure fluctuation influence

The time trace signatures of the flow are synchronized to understand better the influence of the unsteady flow on the axial forces and pressure. The capacitance data (CS1) is shifted to synchronize the flow structure with the force monitoring. This is performed by using the distance between sensors (see Fig. 3, CS1, HQP1, *Fx*,*Fy*, and HQP2) and the structure velocity (v_S). This synchronization facilitates visualization of the influence of dynamic forces in a horizontal elbow in a gas-liquid system. *Fx*, *Fy* forces should be equal if slug momentum has the same value along the slug; however, the result shows that it could change along the slug (especially for pseudo-slug flow).

Figs. 9 and 10 show the pressure and force response traces with the flow structure trace (dimensionless voltage) synchronized at three positions: 1) at the P1 pressure sensor (HQP1), 2) at the elbow (*Fx*,*Fy*), and

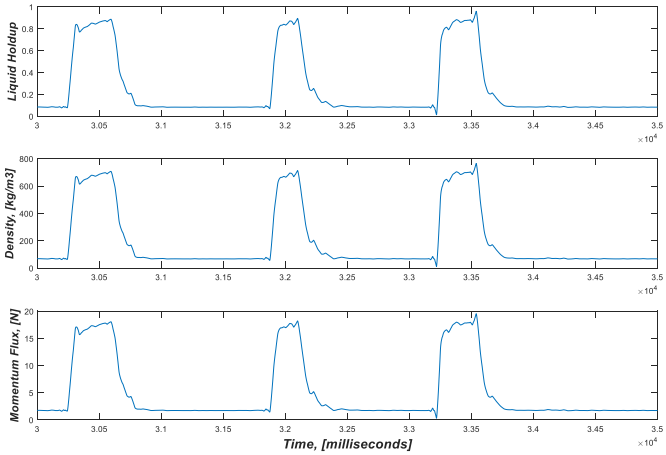

Fig. 7. Sample of two-phase flow monitoring (slug, $v_{SL} = 0.7, v_{SG} = 1.9$ m/s).

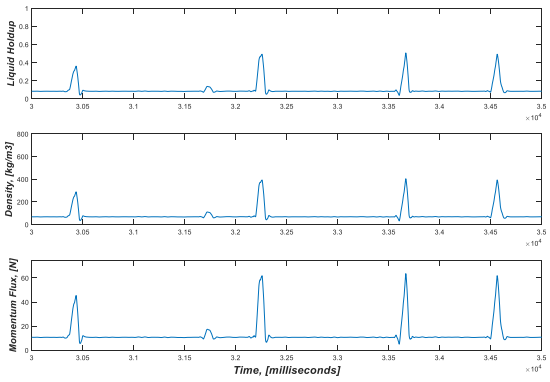

Fig. 8. Sample of two-phase flow monitoring (pseudo-slug, $v_{SL} = 0.7, v_{SG} = 8.2$ m/s).

3) at the P2 pressure sensor (HQP2). This is shown for two flow conditions, one for slug flow and one for pseudo-slug flow. These figures illustrate the response sequence by the flow structures' travel, causing pressure increments and force peaks. For the slug condition the force range is 35 N with pressure fluctuation of 1.03 psi (7080 Pa); for the pseudo-slug condition the force range is 176 N with pressure fluctuation of 4.46 psi (30751 Pa).

Figs. 11 and 12 show the film sequence and slug perturbation periods, combining the force and pressure traces. Pressure is transformed into force by multiplying the transversal area ($P(t)A$) with a value of $A = 0.00203$ m^2; thus, the pressure force fluctuation would be 14.4 N for the slug condition, and 62.4 N for the pseudo-slug condition. Also, the synchronized flow structure traces are included.

During the film region, the force and pressure have the same trends, and the performance could be related mainly to the flow downstream of the test section and changes in the film inventory into the pipe. On the other hand, the slug perturbation starts with the arrival of the slug/pseudo-slug body at the P1 sensor and finishes with the departure from the P2 sensor.

Figs. 13–18 show the progression of the pressure that is expected for the time of the generation of a force peak for different gas flow rates ($v_{SG} = 1.9$, 2.8, 3.6, 5.2, 7.0, and 8.2 m/s), and for a constant liquid flow rate ($v_{SL} = 0.70$ m/s). The samples are extracted within a timeframe of 1 s. The expected elbow pressure progression is built graphically (in black), starting at the time of the beginning of the force peak fluctuation and following the slope of the observed pressure progression for P1 (in blue) and P2 (in orange).

The force peak variation ($\Delta F_x, \Delta F_y$) and elbow pressure fluctuation ($(\Delta P_E)A$) are presented in the graphs. Also, the peak force usually occurs during the progressive increase of the expected elbow pressure. After the arrival of the front of the structure at the elbow, or this peak time, the expected elbow pressure increases a portion (ΔP_P) of the total fluctuation (ΔP_E). This pressure fraction ($\Delta P_P/\ \Delta P_E$) is also presented in the figures and is related to the pressure influence on the force variation; the pressure influence will be bigger when the time of the total pressure progression approaches the time of the force fluctuation. Thus, for the slug flow conditions (Figs. 13–16) the force peaks occurs in 0.04–0.07 s, and the pressure changes requires time in around 0.2–0.3 s; for the pseudo-slug conditions (Figs. 17 and 18) the force peaks occurs in 0.04–0.05 s, and the pressure changes requires similar time in around 0.05–0.07 s.

For low superficial gas velocities, the pressure fluctuations have not reached their maximum value at the time of the peak of force, demonstrating that the peak of hydraulic and pressure forces are not synchronized. As superficial gas velocity increases, the slope of the elbow pressure progression approaches the force signal. For these conditions, the peak of hydrodynamic and pressure forces occurs almost simultaneously. The synchronization on time occurs in the pseudo-slug region.

In slug flow, the force responses have multiple peaks. Usually, the big fluctuation happens at the time of the first jump when the slug body arrives at the elbow. At that time, the momentum term had more relevance than the pressure term (compared with Fig. 1). The expected elbow pressure progression shown in Figs. 13–16 would indicate a low influence in the pressure term in slug flow ($\Delta P_P/\ \Delta P_E < 0.3$). However, for pseudo-slug (Figs. 17 and 18), the pressure term has more relevance ($\Delta P_P/\ \Delta P_E > 0.7$).

As is mentioned in Belfroid et al. (2016), "the force in a 90° bend is given by a pressure and momentum effect (with A, the cross-sectional pipe area) […]. For the transient analysis, we take the transient pressure [$P_P(t)$] and density [$\rho_S(t)$]". To illustrate the momentum and pressure influence on FIV for intermittent flow (SL and PSL), the force range (ΔF_R) can be calculated as follows,

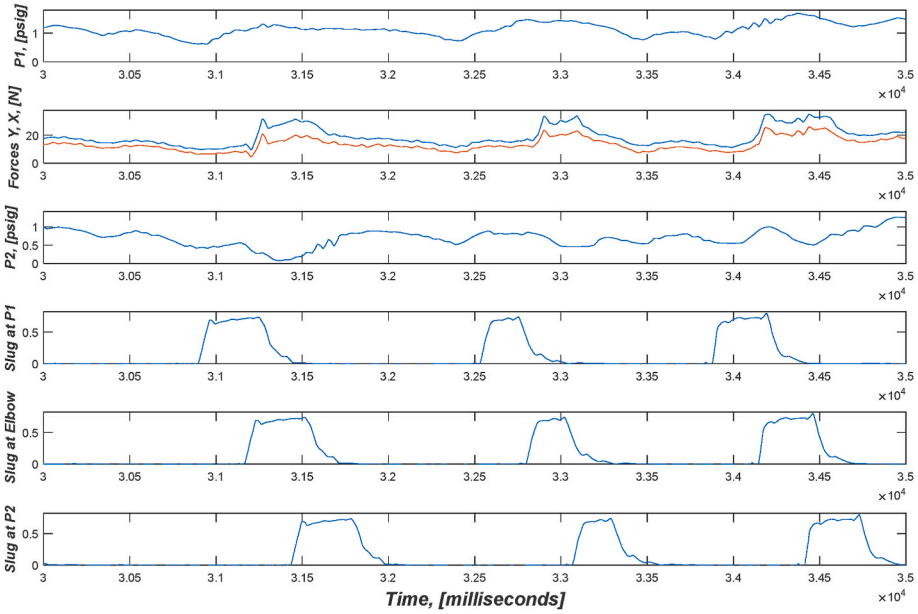

Fig. 9. Two-phase flow trace synchronized (slug, $v_{SG} = 1.9$ m/s, $v_{SL} = 0.7$ m/s).

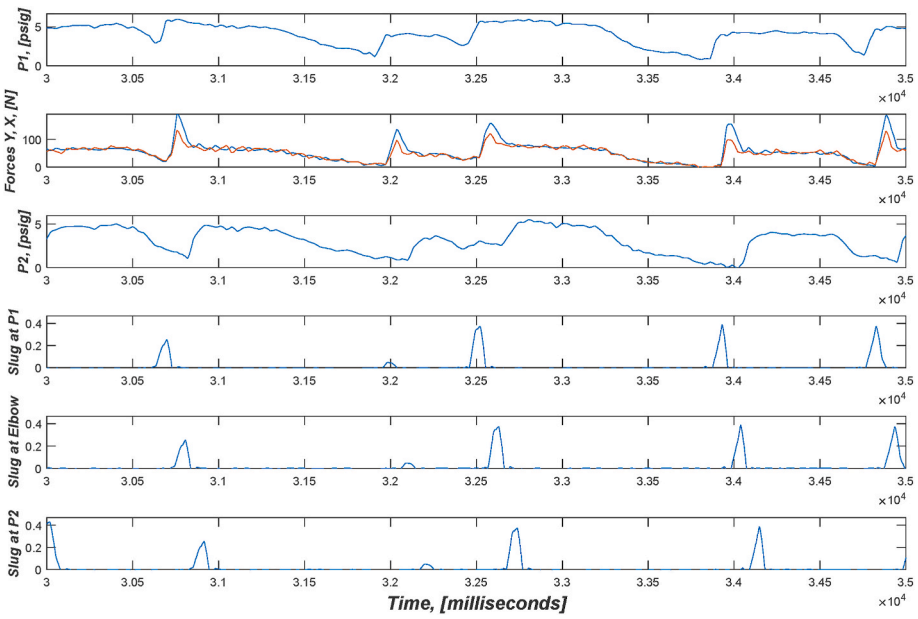

Fig. 10. Two-phase flow trace synchronized (pseudo-slug, $v_{SG} = 8.2$ m/s, $v_{SL} = 0.7$ m/s).

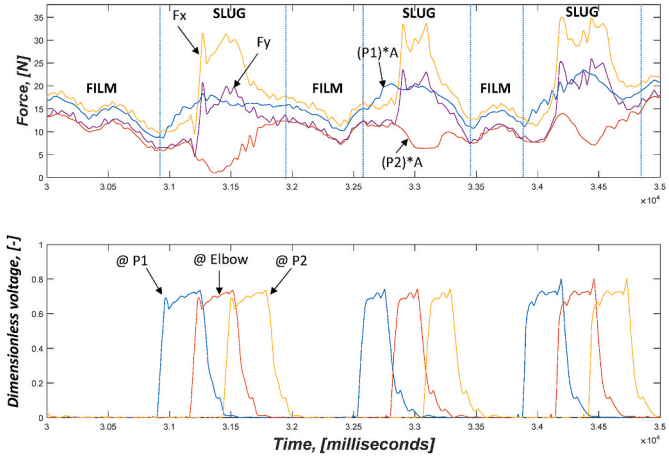

Fig. 11. Flow-induced force and pressure perturbation in a horizontal elbow (slug, $v_{SG} = 1.9$ m/s, $v_{SL} = 0.7$ m/s).

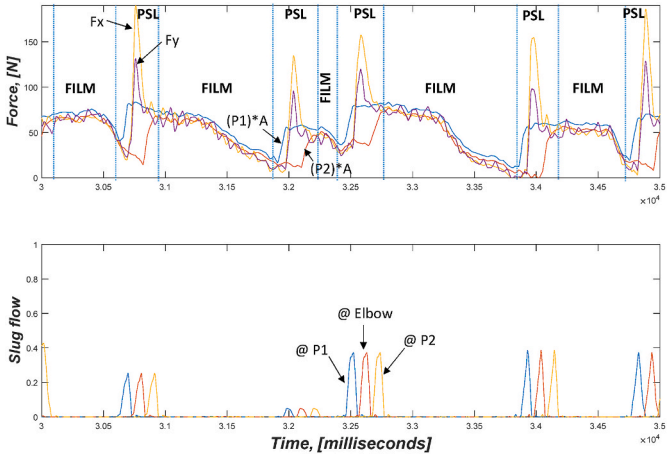

Fig. 12. Flow-induced force and pressure perturbation in a horizontal elbow (pseudo-slug $v_{SG} = 8.2$ m/s, $v_{SL} = 0.7$ m/s).

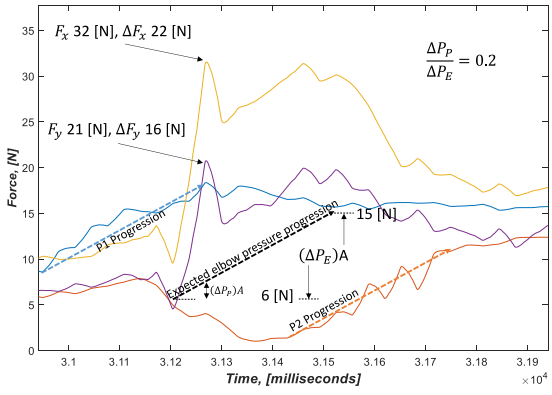

Fig. 13. Elbow pressure progression (slug, $v_{SG} = 1.9$ m/s, $\rho_S v_S^2 A = 18$ N).

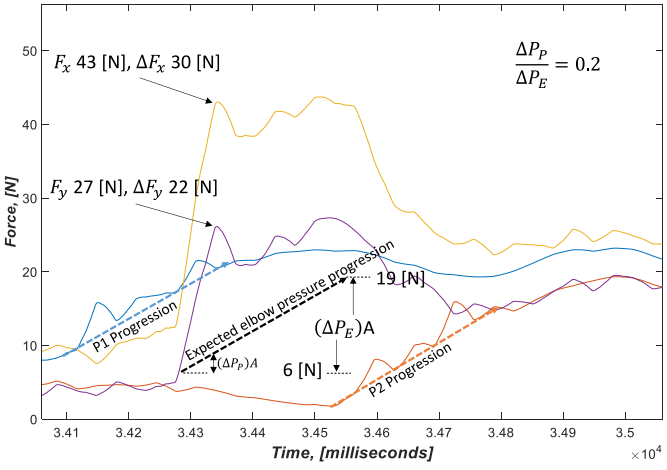

Fig. 14. Elbow pressure progression (slug, $v_{SG} = 2.8$ m/s, $\rho_S v_S^2 A = 25$ N).

$$\Delta F_R(t) = \left(\rho_S(t) v_S^2 + \Delta P_P(t)\right) A\sqrt{2} \tag{3}$$

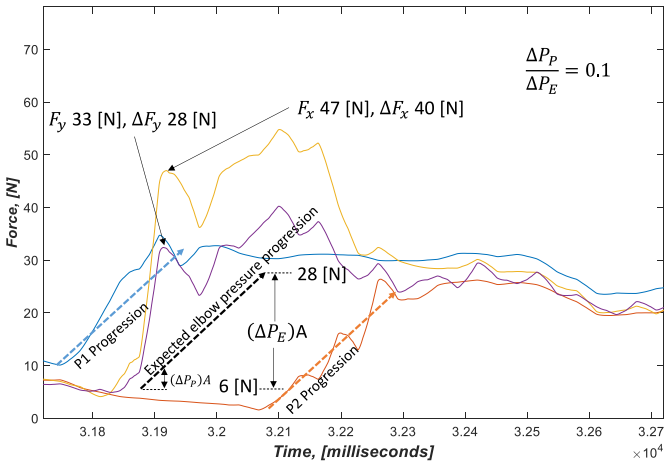

Fig. 15. Elbow pressure progression (slug, $v_{SG} = 3.6$ m/s, $\rho_S v_S^2 A = 33$ N).

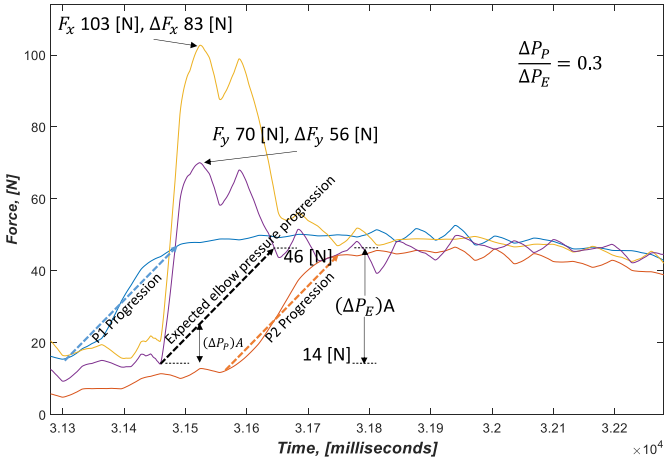

Fig. 16. Elbow pressure progression (slug, $v_{SG} = 5.2$ m/s, $\rho_S v_S^2 A = 48$ N).

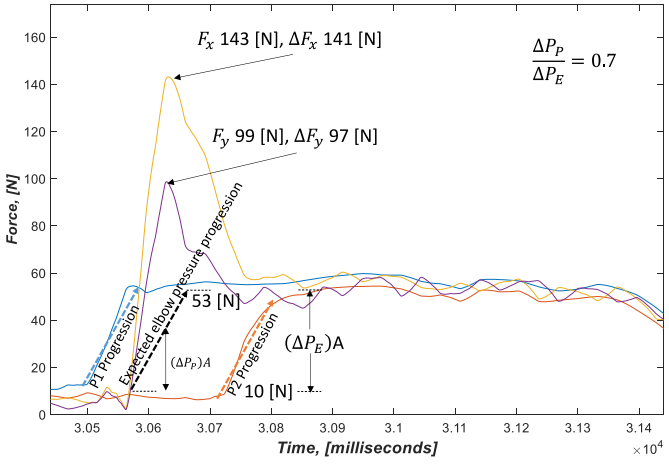

Fig. 17. Elbow pressure progression (pseudo-slug, $v_{SG} = 7.0$ m/s, $\rho_S v_S^2 A = 55$ N).

Assuming that $F_H \approx (\rho_S v_S^2)A$, with a minimal influence of the film region (Garcia et al., 2023a). To visualize the pressure variation influence on data, Figs. 19 and 20 were obtained, with ($\Delta P_P = 0$) and ($\Delta P_P = \Delta P_E$), respectively. The pressure force fluctuation (ΔP_E) was obtained by averaging the fluctuations of the pressure traces (ΔP_1, ΔP_2)

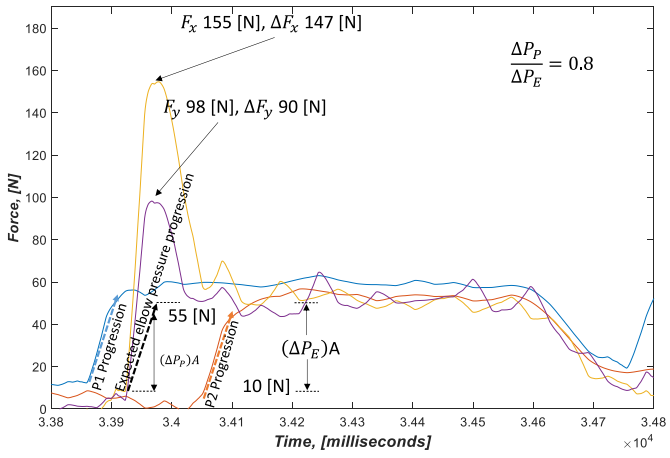

Fig. 18. Elbow pressure progression (pseudo-slug, $v_{SG} = 8.2$ m/s, $\rho_S v_S^2 A = 64$ N).

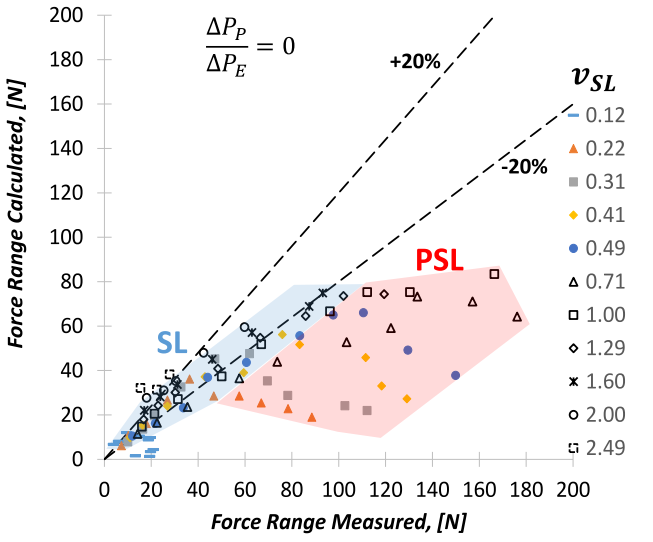

Fig. 19. Prediction of the magnitude of the force peaks. Only the momentum flux term influence.

as the difference between extreme percentiles (P 97.5 and P 2.5) from $P_1(t)$, and $P_2(t)$.

Therefore, comparing the amplitude measurements of the force peaks with the momentum and pressure measured terms suggests the pertinence of the pressure fluctuation on pseudo-slug flow. Here, the pressure varies abruptly for the time the pseudo-slug hits the fitting, adding magnitude at the peak force. On the other hand, the momentum flux term, without the pressure term, is sufficient to explain the magnitude of the force range measured in slug flow. The experimental results agree with previous studies where intermittent flow was accompanied by fluctuations in interrelated variables such as pressure, and momentum flux (Yih and Griffith, 1968), and the influence of those terms on force amplitude (Klinkenberg and Tijsseling, 2021).

4. Model approach and model performance

From this analysis, it is possible to conclude that intermittence of fluid structures induces pressure variations (ΔP_E), characterized by an abrupt increase, and this has an important contribution to the force peak magnitude for pseudo-slug flow, leading to higher peak force amplitudes. Using equation (3), based on Belfroid et al. (2016), it is possible to propose

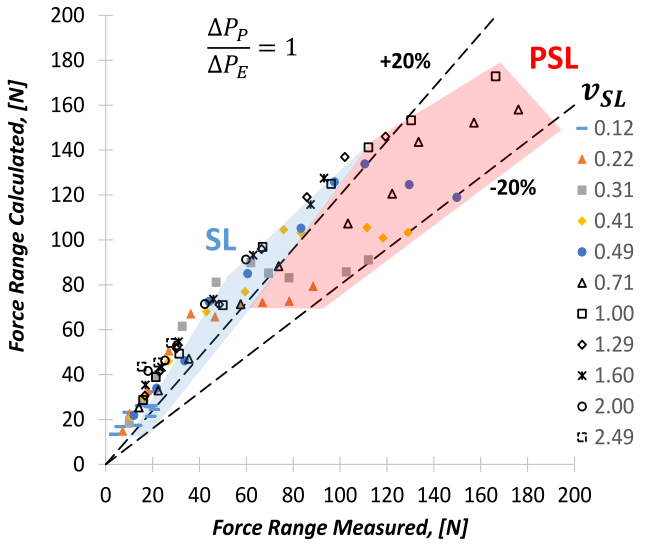

Fig. 20. Prediction of the magnitude of the force peaks. Momentum flux and pressure terms influence.

the next equations for intermittent FIV in a 90° horizontal elbow;

$$\begin{aligned} &\textit{Slug Flow} \\ &\Delta F_R = (\rho_S v_S^2) A\sqrt{2} \\ &\textit{Pseudo} - \textit{slug Flow} \\ &\Delta F_R = (\rho_S v_S^2 + \Delta P_E) A\sqrt{2} \end{aligned} \tag{4}$$

The pressure in the elbow (P_E) increases progressively according to the movement of the structure body as the front changes to the tail (see Fig. 21). The pressure progression is proportional to the size of the body (L_S), and the pressure fluctuation would be the difference in pressure of the body relative to the film flow ($\Delta P_E = \Delta P_{bf}$).

The pressure variation in the elbow caused by the flow of the structure body is assumed to consider the difference between the body pressure gradient and the film pressure gradient. Thus, there is an average pressure gradient along the whole pipeline.

$$\frac{\left(\frac{\Delta P}{l}\Big|_{body}\right) L_S + \left(\frac{\Delta P}{l}\Big|_{film}\right) L_F}{(L_S + L_F)}, \tag{5}$$

The pressure variation would correspond to the maximum deviation of this average line by using the module of

$$\Delta P_{bf} = \left\{ \left(\frac{\Delta P}{l}\Big|_{body}\right) - \frac{\left(\frac{\Delta P}{l}\Big|_{body}\right) L_S + \left(\frac{\Delta P}{l}\Big|_{film}\right) L_F}{(L_S + L_F)} \right\} L_S, \tag{6}$$

It accounts for the pressure change throughout the structure length (L_S)

$$\Delta P_{bf} = \left(\frac{L_F}{(L_S + L_F)}\right) L_S \left(\frac{\Delta P}{l}\Big|_{body} - \frac{\Delta P}{l}\Big|_{film}\right), \tag{7}$$

where the pressure gradients of the body and the film regions could be obtained from the mechanistic model proposed by Zhang et al. (2003). These pressure gradients are obtained with multiphase flow parameters (friction and gravity) upstream of the fitting (elbow). Instead of L_S, another equivalent length that could be considered is $L_F(L_B/Ls)$, which includes the influence of the bend length (L_B)

$$\begin{aligned} \frac{\Delta P}{l}\Big|_{body} &= \frac{\tau_{Mix} S}{A} + [\rho_L H_{LLS} + \rho_G (1 - H_{LLS})] g \sin\theta, \frac{\Delta P}{l}\Big|_{film} = \frac{\tau_{GW} S_G}{A} + \frac{\tau_{LW} S_L}{A} \\ &+ [\rho_L H_{LF} + \rho_G (1 - H_{LF})] g \sin\theta \end{aligned} \tag{8}$$

Where H_{LLS} is the slug holdup, H_{LF} is the liquid film holdup, τ_{GW} is the film gas shear stress, τ_{LW} is the film liquid shear stress, τ_{Mix} is the slug mixture shear stress, S_G is the gas perimeter, and S_L is the liquid film perimeter. All flow parameters are obtained using Zhang et al. (2003). S and A are the pipe perimeter and cross-sectional area, respectively.

The performance of the model approach was evaluated using available data for pressure variation in the elbow test section ($\Delta P_E < 5\,psi$) and using the TUFFP Unified Model, as detailed in Fig. 22. It is worth highlighting that the inclination angle is zero ($\theta = 0$), resulting in only dynamic pressure gradients. There is a clear underprediction ($\Delta P_E < 1.5\,psi$) although the coefficient of determination is acceptable ($R^2 = 0.86$), showing a fair assessment of the variables selected for the model (body pressure gradient, film pressure gradient, and structure length). From the linear regression, the underprediction tends to be one-quarter of the measured pressure fluctuation in a straight pipe. Based on this, it is suggested that the maximum pressure fluctuation in the elbow is estimated as four times the pressure drop in the straight pipe.

The magnitude of the pressure fluctuation could also be related to the change in the dynamic head (i.e. $\rho v^2/2$) due to the alternative nature of slug and film flow; as mentioned by Yih and Griffith (1968), "intermittent flow is accompanied by severe pulsations in pressure, void fraction, and momentum fluxes; these time-varying quantities are interrelated, and measurements of the fluctuation in either one of them would lead to

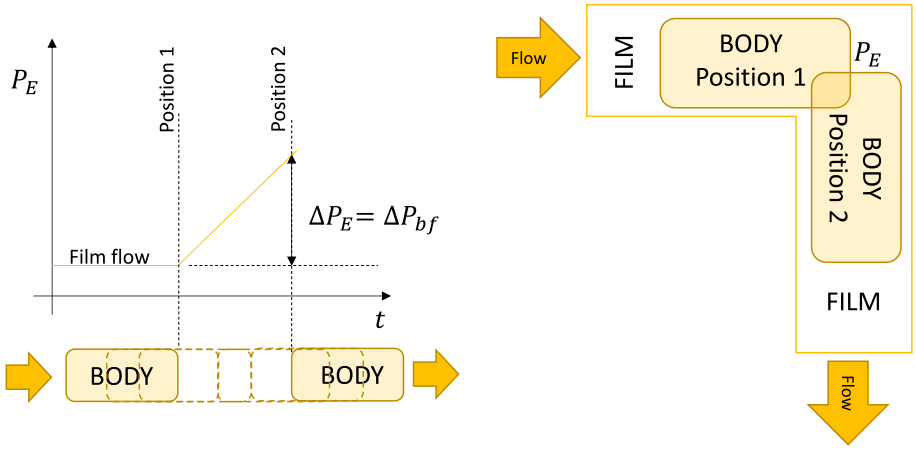

Fig. 21. Change in elbow pressure by structure body flow.

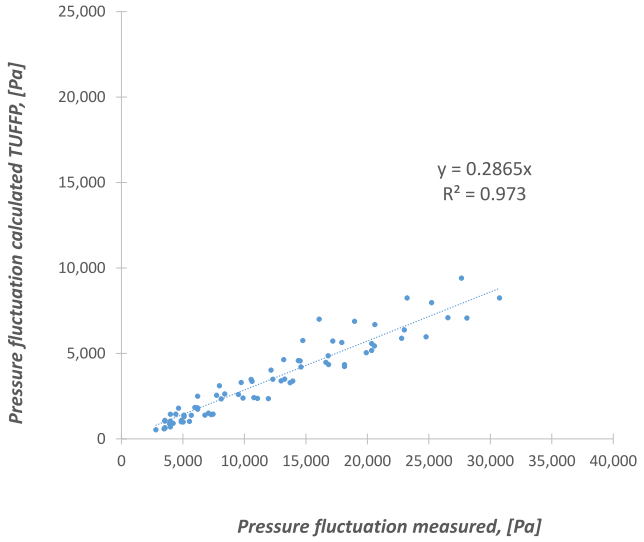

Fig. 22. Pressure fluctuation structure to film prediction (TUFFP Unified Model).

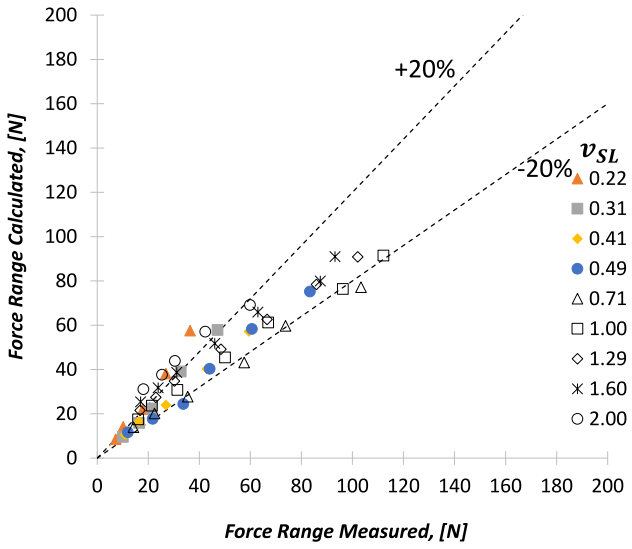

Fig. 23. Magnitude of force peak (TUFFP Slug model). AARE 18%.

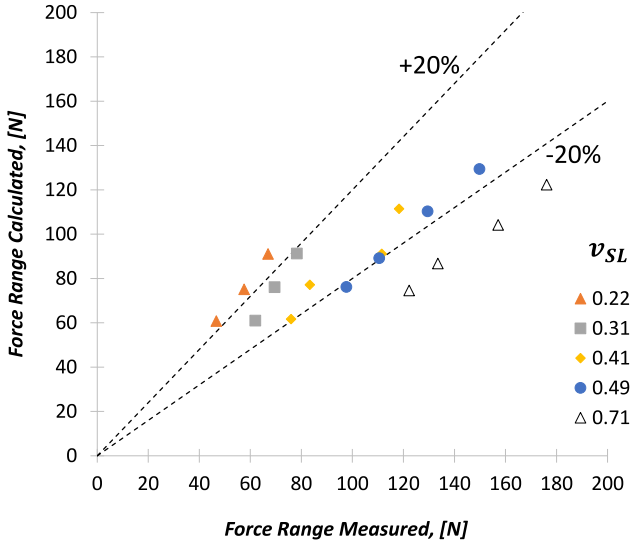

Fig. 24. Magnitude of force peak (TUFFP Pseudo-slug model). AARE 21%.

the understanding of the others." Thus, more analysis is recommended to understand those interactions better and possibly improve the modeling of pressure fluctuation.

Other suggestions can be made to improve the model's performance in future studies, such as the usage of different friction closures, consideration of the fitting or bend (L_B) flow resistance, improvement of the prediction of the structure length, and/or expansion of the body pressure gradient by including interfacial shear stress. Most of the closure relationships has been developed for slug flow, and new considerations need to be included for pseudo-slug flow.

4.1. Magnitude of force peak modeling

The prediction of unbalanced forces is based on the identification of intermittent flow. Mechanistic modeling is recommended for calculating flow parameters required in determining momentum flux and pressure fluctuation. A code based on the Modified Unit Cell Model has been used (Soedarmo, 2019) for pseudo-slug conditions. The magnitude of the force peak has been evaluated using FIV force measurements, together with the TUFFP-slug model (Zhang et al., 2003) and the TUFFP-pseudo-slug model (Soedarmo, 2019).

The force magnitude prediction considers the findings of the modeling effort for structure velocity (v_S), structure density (ρ_S), and pressure fluctuation (ΔP_{bf}). The selection of these closures influences the results. In this evaluation, the selections for the closure relationships are provided in Table 2.

Table 2
Model predictivity on different flow configurations (oil systems).

Closure relationships	Slug Model	Pseudo-slug Model
Wettability	Zhang and Sarica (2011)	Zhang and Sarica (2011)
Maximum Entrainment	0.75	0.75
Entrainment	Zhang et al. (2003)	Zhang et al. (2003)
Interfacial Friction	Zhang et al. (2003)	Zhang et al. (2003)
Wall Friction	Churchill (1977)	Churchill (1977)
Mixture Friction	Churchill (1977)	Churchill (1977)
Slug Length	Zhang et al. (2003)	Zhang et al. (2003)
Slug Body Holdup	Gregory et al. (1978)	Soedarmo (2019)
Drift Velocity	Zhang et al. (2003)	Zhang et al. (2003)
Translational Velocity	Zhang et al. (2003)	Zhang et al. (2003) and structure velocity correction (Garcia et al., 2023c)

The force range of the peaks has been calculated for 53 SL flow conditions, including only the momentum flux term from the mechanistic model's results. Fig. 23 presents the performance of the mechanistic modeling to predict force peak magnitude. The results are shown for different superficial liquid velocities. The average absolute relative error is 18% for all the SL flow conditions.

For 18 PSL flow conditions, the force range of the peaks, including the momentum flux and pressure terms, was calculated using the results of the mechanistic pseudo-slug model. Fig. 24 presents the performance of the mechanistic modeling to predict force peak magnitude. The results are shown for different superficial liquid velocities. The average absolute relative error is 21% for all the PSL flow conditions.

Fig. 25 shows the force prediction using only the momentum term to illustrate the importance of including the pressure influence for PSL conditions. The performance deteriorates, and the AARE increases from 21 to

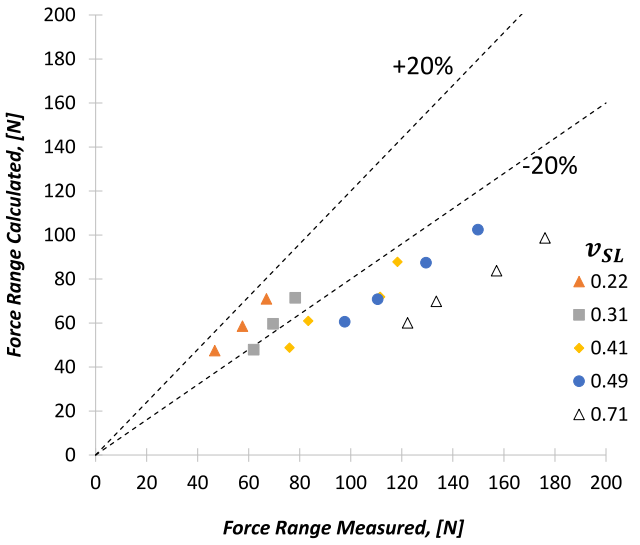

Fig. 25. Magnitude of force peak without pressure influence (TUFFP Pseudo-slug model). AARE 28%.

28%.

As previously mentioned, there is room to improve the pressure fluctuations and the force range for PSL flow conditions (see Fig. 25). Yet, important developments have been made for multiphase variables associated with FIV in pipe systems.

The present work proved that it is possible to predict more accurately one of the critical parameters used to determine the fatigue of piping systems due to multiphase flow: the range of stress or the magnitude of the force peaks caused by the impact of fluid structures on the accessories.

5. Concluding remarks

Pseudo-slug flow leads to more severe force peaks, which could result in more pronounced structural vibration. This happens during the transition from slug flow to annular flow, with high flow velocity and moderate structure density. The flow and hitting of slug/pseudo-slugs are causing the force peaks.

Analysis of the elbow pressure progression indicates a low change in the pressure term for the time of the force peak occurrence in slug flow. Although, in slug flow, the force responses have multiple peaks, usually, the big fluctuation happens at the time of the first jump when the slug body arrives at the elbow. Thus, the momentum flux term had more relevance for slug flow than the pressure term.

However, for pseudo-slugs, the pressure term has more significance. Under these conditions, the pressure variation, characterized by an abrupt increase, has an important contribution to the force peak magnitude for pseudo-slug flow, leading to higher peak force amplitudes. Therefore, the multiphase variables required to be modeled related to force peak magnitude are structure density, structure velocity, and pressure variation.

Nomenclature

d	pipe diameter, m
μ_S	slug viscosity, Pa.s
H_L	in-situ liquid holdup
H_{LLS}	slug liquid holdup
v_S	structure velocity, m/s
v_M	mixture velocity, m/s
v_{SL}	liquid superficial velocity, m/s
v_{SG}	gas superficial velocity, m/s
ρ_L	liquid density, kg/m^3
ρ_G	gas density, kg/m^3
ρ_S	structure density, kg/m^3
A	pipe cross-sectional area, m^2
F_x	X-direction overall force, N
F_y	Y-direction overall force, N
F_H	hydrodynamic force, N
F_R	resultant force, N
ΔF_R	force range magnitude, N
P_E	elbow pressure, psig
ΔP_E	elbow pressure fluctuation, psig
ΔP_P	elbow pressure portion, psig

CRediT authorship contribution statement

C. Garcia: Writing – review & editing, Writing – original draft, Validation, Investigation, Data curation, Conceptualization. **C. Nogueira Sondermann:** Writing – review & editing, Validation, Methodology, Investigation, Formal analysis. **E. Pereyra:** Writing – review & editing, Validation, Supervision, Project administration, Investigation, Formal analysis, Data curation, Conceptualization. **L. Korelstein:** Writing – review & editing, Validation, Investigation, Formal analysis, Data curation. **C. Sarica:** Writing – review & editing, Validation, Supervision, Resources, Project administration, Methodology, Investigation, Funding acquisition, Formal analysis, Conceptualization.

Declaration of competing interest

The authors declare that they have no known competing financial interests or personal relationships that could have appeared to influence the work reported in this paper.

Acknowledgments

TUFFP members are acknowledged for their support of this project. In addition, Mr. Scott Graham, Mr. Jose Aramburu, and Mr. Luis Sanchez of The University of Tulsa are acknowledged for their important contributions to the construction of the experimental facility.

Data availability

Data will be made available on request.

References

ASTM D341-09, 2015. Standard Practice for Viscosity-Temperature Charts for Liquid Petroleum Products, vol. 125. ASTM International, pp. 266–273, 2015.

Barnea, D., 1987. A unified model for predicting flow-pattern transitions for the whole range of pipe inclinations. Int. J. Multiphas. Flow 13 (1), 1–12, 1987.

Belfroid, S.P.C., Nennie, E., Lewis, M., 2016. "Multiphase forces on bends-large scale 6" experiments. In: Proceedings of the TNO and Xodus Group, SPE-181604-MS, SPE Annual Technical Conference and Exhibition Held in Dubai. UAE, pp. 26–28. September (2016).

Brito, R., 2012. Effect of medium oil viscosity on two-phase oil-gas flow behavior in horizontal pipes. Thesis of Master of Science in Petroleum Engineering. The University of Tulsa. The Graduate School (2012).

Dieck, R.H., 2007. Measurement Uncertainty: Methods and Applications, 4th ed. ISA, The Instrumentation, System, and Automation Society, Printed USA, pp. 39-60. (2007).

Garcia, C., Nemoto, R., Pereyra, E., Korelstein, L., Sarica, C., 2023a. Hydrodynamic forces in a horizontal-horizontal elbow in a gas-liquid system. Int. J. Multiphas. Flow 159 (February 2023), 104321. https://doi.org/10.1016/j.ijmultiphaseflow.2022.104321, 2023.

Garcia, C., Pereyra, E., Sarica, C., Korelstein, L., 2023b. An improved unified correlation for prediction of slug frequency in gas-liquid flow. Paper Presented at the 20th International Conference on Multiphase Production. Nice, France, 26th -28th June, (2023.

Garcia, C., Nogueira Sonderman, C., Pereyra, E., Sarica, C., 2023c. A novel approach to predict hydrodynamic forces using a mechanistic model for pseudo-slug flow. Paper Number: SPE-214972-MS, Presented at the SPE Annual Technical Conference and Exhibition, San Antonio, Texas, USA, October (2023).

Gottfried, B.S., 1965. A mathematical model of thermal oil recovery in linear systems. Society of Petroleum Engineers Jornal, SPE 1117, Paper Presented at SPE Production Research Symposium Held. Tulsa, OK, May 3-4 (1965.

Klinkenberg, A.M., Tijsseling, A.S., 2021. Stochastic mechanistic modeling of two-phase slug flow forces on bends in horizontal piping. Int. J. Multiphas. Flow 144, 103778. https://doi.org/10.1016/j.ijmultiphaseflow.2021.103778, 2021.

Liu, Y., Miwa, S., Hibiki, T., Ishii, M., Morita, H., Kondoh, Y., Tanimoto, K., 2012. Experimental study of internal two-phase flow induced fluctuating force on a 90° elbow. Chem. Eng. Sci. 76, 173–187, 2012.

Miwa, S., Hibiki, T., 2020. State-of-the-art in plant component flow-induced vibration (FIV). Exp. Comput. Multiph. Flow 2 (1), 1–12, 2020.

Shoham, O., 2006. Mechanistic modeling of gas-liquid two-phase flow in pipes. SPE Book. Society of Petroleum Engineers, printed in the USA, 2006.

Soedarmo, A., 2019. Gas-Oil Flow in Upward-Inclined Pipes: Pseudo-slug Flow Modeling and Upscaling Studies. University of Tulsa, Tulsa, Oklahoma, USA. Ph.D. dissertation.

Tay, B.L., Thorpe, R.B., 2014. Hydrodynamic forces acting on pipe bends in gas-liquid slug flow. Chem. Eng. Res. Des. 92, 812–825, 2014.

Yih, T.S., Griffith, P., 1968. Unsteady momentum fluxes in two-phase flow and the vibration of nuclear reactor components. Department of Mechanical Engineering, MIT, Cambridge, Massachusetts.

Zhang, H.Q., Wang, Q., Sarica, C., Brill, J.P., 2003. Unified model for gas-liquid pipe flow via slug dynamics – Part 1: model development. ASME J. Energy Resour. Technol. 125, 266–273.